Phonon properties, polymorphism, and amorphization of $Dy_2Mo_4O_{15}$ under high hydrostatic pressure

W. Paraguassu,[1,*] M. Maczka,[2] A. G. Souza Filho,[3] P. T. C. Freire,[3] J. Mendes Filho,[3] and J. Hanuza[4]
[1]*Departamento de Fisica, Universidade Federal do Maranhão, São Luis 65085-580, MA, Brazil*
[2]*Institute of Low Temperature and Structure Research, Polish Academy of Sciences, P.O. Box 1410, 50-950 Wroclaw 2, Poland*
[3]*Departamento de Fisica, Universidade Federal do Ceara, P.O. Box 6030, Fortaleza 60455-970, CE, Brazil*
[4]*Department of Bioorganic Chemistry, University of Economics, 53-345 Wroclaw, Poland*
(Received 15 July 2010; revised manuscript received 27 September 2010; published 11 November 2010)

$Dy_2Mo_4O_{15}$ crystal was investigated by high-pressure Raman spectroscopy experiments. The assignment of vibrational modes at ambient pressure was made based on lattice-dynamics calculations and the results helped us also to discuss high-pressure transformations observed in this material. A pressure-induced structural phase transition was observed at about 2.0 GPa. This transition is associated with significant rearrangement of the molybdenum-oxygen sublattice and an increase in the molybdenum-oxygen coordination most likely changing from tetrahedral to pentagonal. The bond compressibility, related to the Mo-O bonds, were estimated for both $P2_1/c$ and high-pressure phase. Upon further increase in pressure $Dy_2Mo_4O_{15}$ exhibits irreversible amorphization above 4.7 GPa. The irreversible character of this transformation points out to either chemical decomposition or crystallographic transformation as a cause of this amorphization process. Our analysis suggests that the amorphization of $Dy_2Mo_4O_{15}$ may be most likely attributed to a chemical decomposition.

DOI: 10.1103/PhysRevB.82.174110 PACS number(s): 81.40.Vw, 78.30.Ly, 78.30.Hv, 63.20.D−

I. INTRODUCTION

$Dy_2Mo_4O_{15}$ (DMO) belongs to a class of lanthanide molybdates that exhibit ferroelectric/ferroelastic properties, negative thermal expansion, catalytic properties, and fast oxide-ion conduction.[1–4] $Ln_2Mo_4O_{15}$ molybdates (*Ln* =lanthanide) crystallize in four different structures: I for *Ln*=La ($P2_1/n$ space group), II for *Ln*=Ce, Pr ($P\bar{1}$ space group with $\{Mn_4O_{14}\}_\infty$ groups), III for *Ln*=Nd-Gd ($P\bar{1}$ space group with $\{Mn_4O_{17}\}_\infty$ and MoO_4 groups), and IV for *Ln* =Tb-Lu ($P2_1/c$ space group).[3–6] Negative thermal expansion (NTE) was discovered only for the structural type IV.[7] For instance, it was shown that DMO exhibits NTE in the 25–170 °C temperature range followed by a positive thermal expansion above 170 °C.[7] The structure of this material consists of Mo_2O_7 units that are weakly connected to MoO_4 tetrahedra.[7] This structural framework is similar to ZrV_2O_7 which consists of V_2O_7 units and $Zr(WO_4)_2$ built up of two weakly connected WO_4 tetrahedra.[7] Both materials exhibit NTE phenomena.

There is a number of works reporting high-pressure Raman and structural studies of $Ln_2(MoO_4)_3$ molybdates. However, to the best of our knowledge $Ln_2Mo_4O_{15}$ molybdates have not been yet the subject of spectroscopic studies and this paper reports high-pressure experiments in the $Ln_2Mo_4O_{15}$ system. Previous high-pressure works on $Ln_2(MoO_4)_3$ reported observation of pressure-induced amorphization (PIA) in these systems. It has been proposed based on computer simulation studies that NTE and PIA have common origin in framework structures (tetrahedral bonded networks).[8] This model has been argued to be also valid for tetrahedral-octahedral network structures.[9]

It was observed that PIA is an irreversible process in some cases while in other cases, depending on physical system and experimental conditions, this process can be reversible. There is a number of reports of different materials presenting PIA attributed to different mechanisms, namely, (a) mechanical deformation; (b) hindrance of equilibrium phase transition, or (c) chemical decomposition.[10–12] Reports on pressure-induced decomposition of $Ln_2(MoO_4)_3$ systems into a mixture of simple oxides at high temperature and high pressure, and the observation of PIA at ambient temperature suggested that in these systems, PIA could arise from the kinetic hindrance of an equilibrium decomposition.[11–15] For decomposition to occur at high pressure, it is necessary that the total volume of the daughter phases is less than that of the parent phase. A calculation of the volume change (δV) for a number of compounds exhibiting PIA has suggested negative δV as a new criterion for predicting PIA at ambient temperature.[11] By this analyses, other members of the family of tungstates and molybdates such as $Hf(WO_4)_2$, $Zr(MoO_4)_2$, $Sc_2(MoO_4)_3$, and $Y_2(WO_4)_3$, which have been reported to exhibit NTE over a limited range of temperature, are likely candidates for a possible decomposition when subjected to suitable conditions.[16–21]

PIA is an important but still poorly explored subject of high-pressure research. We expect that the present work will help to better understand this intriguing phenomenon. The main aim of this work is to study pressure-induced polymorphism and PIA for DMO under hydrostatic pressure conditions. To achieve this goal we have measured the Raman spectra of DMO system in the 0.1–10.1 GPa range and performed phonon calculations to make a complete and definite mode assignment for this system.

II. EXPERIMENTAL

DMO was synthesized by firing stoichiometric mixture of Dy_2O_3 and MoO_3 at 600 °C for 24 h, followed by regrinding of the obtained material and subsequent firing at 700 °C for 24 h. The purity of the synthesized DMO was checked by x-ray powder diffraction method.

TABLE I. Correlation diagram between the molecular (D_{3d}), site (C_i), and factor group symmetries (C_{2h}). Assignment is based on Ref. 22. ν=stretching; δ=bending; ρ=rocking; τ=torsion; s=symmetric, as =asymmetric; and b=bridge.

Molecular symmetry D_{3d}	Site symmetry C_i	Factor group Symmetry C_{2h}	Assignment
A_{1g}	A_g	A_g+B_g	$\nu_s MoO_3$
A_{1g}	A_g	A_g+B_g	$\delta_s MoO_3$
A_{1g}	A_g	A_g+B_g	ν_sMo-O_b
E_g	$2A_g$	$2A_g+2B_g$	$\nu_{as} MoO_3$
E_g	$2A_g$	$2A_g+2B_g$	$\delta_{as} MoO_3$
E_g	$2A_g$	$2A_g+2B_g$	$\rho_s MoO_3$
A_{1u}	A_u	A_u+B_u	τ_sOMo-MoO
A_{2u}	A_u	A_u+B_u	$\nu_s MoO_3$
A_{2u}	A_u	A_u+B_u	ν_{as}Mo-O_b
A_{2u}	A_u	A_u+B_u	$\delta_s MoO_3$
E_u	$2A_u$	$2A_u+2B_u$	$\nu_{as} MoO_3$
E_u	$2A_u$	$2A_u+2B_u$	$\delta_{as} MoO_3$
E_u	$2A_u$	$2A_u+2B_u$	$\rho_{as} MoO_3$
E_u	$2A_u$	$2A_u+2B_u$	δMo-O_b-Mo

The pressure-dependent Raman spectra were obtained with a Jobin-Yvon T64000 spectrometer operating in the double-subtractive mode, equipped with a N_2-cooled charge-coupled-device detection system. The 532 nm line of a diode-pumped solid-state laser was used as the excitation. An Olympus microscope lens with a focal distance f =20.5 mm and numeric aperture NA=0.35 was used to focus the laser beam on the sample surface. High-pressure Raman experiments were performed at room temperature using a diamond-anvil cell with Nujol as the transmitting fluid. The pressure calibration was achieved by using the well-known pressure shift of the ruby luminescence lines. The spectrometer slits were set for a resolution of 2 cm^{-1}.

III. RESULTS AND DISCUSSION

A. Lattice-dynamics calculations

We first discuss the vibrational properties of DMO at ambient pressure aiming to get understanding of the basic properties and get insights under its behavior under high pressure. As mentioned above, the structure of DMO consists of Mo_2O_7 units that are weakly connected to MoO_4 tetrahedra. Site symmetry of the MoO_4 and Mo_2O_7 units is C_1 and C_i, respectively. A standard group theoretical analysis for the $P2_1/c$ structure of DMO containing 42 atoms in the unit cell leads to 136 degrees of freedom at the Brillouin-zone center (Γ point). The optical modes are distributed among the irreducible representations of the factor group C_{2h} as $30A_g+30B_g+32A_u+31B_u$. Selection rules state that A_g and B_g modes are Raman active whereas the A_u and B_u modes are infrared (IR) active. These modes can be further subdivided into translational, librational, and internal modes. Since the unit cell comprises four Dy, four MoO_4, and two Mo_2O_7 units, these units give rise to $3A_g+3B_g+3A_u+3B_u$, $3A_g+3B_g+3A_u+3B_u$, and $3A_u+3B_u$ translational modes, respectively. It should be remembered, however, that among these translational modes three modes (A_u+2B_u) belong to the acoustic branches. The number of librational modes is $3A_g+3B_g+3A_u+3B_u$ and $3A_g+3B_g$ for MoO_4 and Mo_2O_7, respectively. $9A_g+9B_g+9A_u+9B_u$ internal modes of the MoO_4 tetrahedra can be subdivided into ν_1 symmetric stretching ($A_g+B_g+A_u+B_u$), ν_3 antisymmetric stretching ($3A_g+3B_g+3A_u+3B_u$), ν_2 symmetric bending ($2A_g+2B_g+2A_u+2B_u$), and ν_4 antisymmetric bending modes ($3A_g+3B_g+3A_u+3B_u$). Situation is more complicated in the case of Mo_2O_7 units. The Mo-O-Mo bridge in the Mo_2O_7 unit of DMO is linear and the bridging oxygen atom is located on inversion center.[4] Therefore the number of internal modes can be derived assuming D_{3d} symmetry for the free Mo_2O_7 unit. For this symmetry, the 21 internal modes of the Mo_2O_7 unit are distributed among $3A_{1g}+3E_g+A_{1u}+3A_{2u}+4E_u$ irreducible representations.[22] In the DMO crystal these modes will give rise to $9A_g+9B_g+12A_u+12B_u$ internal modes (see the correlation diagram presented in Table I).

As one can notice, phonon properties of DMO are very complicated. Therefore in order to get insight into these properties, we have performed lattice-dynamics calculations for the room temperature $P2_1/c$ structure. These calculations were performed using GULP code developed by Gale.[23] We have determined a set of classical ionic pair potential that better optimize the DMO structure. The obtained set of potential parameters has been then used to derive the initial force constants that were refined using Wilson's FG matrix method and the software package VIBRATZ developed by Dowty.[24]

The ionic shell model used in the GULP code treats the material as a collection of core-shell systems (accounting for nuclei and electron shell) interacting to each other through electrostatic and short-range classic potentials. This model was successfully used for a number of molybdate- and tungstate-based systems.[25–28] The following interatomic potential is taken into account,

TABLE II. Potential parameters [see Eq. (1) in the text] and ionic charges used in the lattice-dynamics calculation.

Buckingham			
Shell-shell	b (eV)	ρ (Å)	c (eV Å^6)
Mo-O	1385.2	0.375	0
Dy-O	16.19×10^6	0.14	0
O-O	22764	0.149	27.879
Three body			
Core-shell-shell	k	θ	
Mo-O-O	5.09	100	
Charges			
Core	Core	Shell	
$Z_{Tb}=3$	$Z_{Mo}=6$	$Z_O=-2.84819$	
Spring			
$k_O=74.92$			

$$U_{ij}(r_{ij}) = \frac{z_i z_j e^2}{r_{ij}} + b_{ij}\exp\left[\frac{-r_{ij}}{\rho_{ij}}\right] - \frac{c_{ij}}{r_{ij}^6}. \quad (1)$$

The first term is related to the Coulomb forces for modeling the long-range interactions. The second term is related to the Born-Mayer-type repulsive interaction for accounting the short-range forces. A van der Waals attractive interaction (third-term) models the dipole-dipole interaction. z_i and z_j are the effective charges of the i and j ions, respectively, separated by the distance r_{ij}. The parameters ρ_{ij} and b_{ij} correspond to the ionic radii and ionic stiffness, respectively. The initial lattice parameters and atomic positions for the DMO structure were taken from the experimental data.[7,29] The optimized potential parameters and ionic charges obtained after energy minimization are listed in Table II. By using this set of parameters, a good agreement between the calculated and experimental lattice parameters for the $P2_1/c$ space group was obtained (see Table III).

The phonon calculations were performed using Wilson's FG matrix method and the software package VIBRATZ developed by Dowty.[24] The initial force constants were obtained by using the relation

$$f_{ij} = -\frac{1}{r}\frac{\partial U_{ij}(r)}{\partial r}, \quad (2)$$

where the indices i and j refer to interacting ions, and r is the distance between them. In order to better fit the experimental data, the obtained force constant values for the Mo-O bonds were refined. This procedure is necessary in order to correct the lack of covalence in the ionic model. In the Fig. 1 we show the calculated wave numbers vs Mo-O distance for the A_g modes (open squares) along with the observed experimental wave numbers (solid circles). Note that the refinement was made in a way that the calculated wave numbers for the Mo-O stretching modes follow an exponential dependence on the Mo-O distance. This behavior was observed for a number of molybdenum oxides and follows from the empirical model, which correlates a stretching frequency with a bond length,[30]

TABLE III. Calculated and observed lattice parameters.

Cell parameter	$P2_1/c$ Experimental	$P2_1/c$ Calculated
Volume	664.2917	665.2994
a	6.823	6.842331
b	9.607	9.607203
c	10.524	10.58724
α	90	90
β	105.64	107.0702
γ	90	90

$$\nu = \nu_0 + Ae^{-r/B}. \quad (3)$$

The parameters $\nu_0=709.8$ cm^{-1}, $A=95177.8$ cm^{-1}, and B $=0.2709$ Å, were obtained from exponential fitting. A complete list of the calculated (IR and Raman) and experimental Raman modes along with the proposed assignment is presented in Table IV.

The performed calculations show that the Raman bands in the 783–970 cm^{-1} range correspond to stretching vibrations of the MoO_4 tetrahedra and Mo_2O_7 groups. They also show that the antisymmetric modes of the Mo-O-Mo bridge in the Mo_2O_7 units should be observed only in the IR spectrum at about 1000 cm^{-1}. Symmetric stretching and bending mode

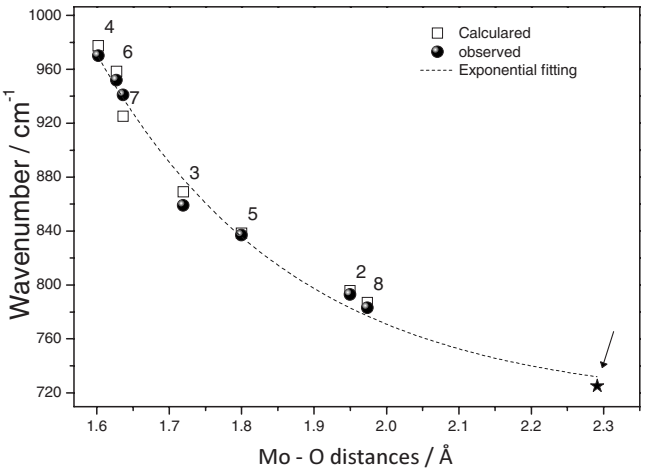

FIG. 1. Calculated wave numbers vs Mo-O distance for the A_g modes (open squares) along with the observed wave numbers (solid circles). The star point refers to the 721 cm^{-1} stretching mode observed above 2 GPa. The numbers over the points correspond to those oxygen atoms, which most significantly contribute to the respective vibration (labels follow the literature Ref. 4).

TABLE IV. Calculated (Raman and IR) and observed (Raman) wave numbers for DMO (ambient pressure phase) together with the proposed assignment.

Calculated (cm^{-1})				Observed (cm^{-1})	Assignment
A_g	B_g	A_u	B_u		
		1004	1004		ν_{as}Mo-O_b
977	977	976	977	970	$\nu_1(MoO_4)+\nu_sMoO_3$
958	958	960	960	952	
919	924	919	924	941	
869	862	869	862	859, 844	$\nu_{as}MoO_3$
838	837	838	837	837, 835	$\nu_{as}MoO_3$
796	795	803	804	813	$\nu_3(MoO_4)$
787	786	779	779	793, 783	$\nu_3(MoO_4)$
410	415	424	421	409	bending modes [δ_sMoO_3, $\delta_{as}MoO_3$,
373	365	383	384	396	$\nu_2(MoO_4)$, and $\nu_4(MoO_4)$]
362	359	360	366	367	
340	328	344	349	351	
329	314	326	317	319	
308	305	296	308	301	
266	261	283	274	283	
257	254	272	266		
275	273			271	ν_sMo-O_b
		249	256	241	$\rho_{as}MoO_3$ and $L(MoO_4)$
235	248	235	233	221	
216	231	228	229	191	
211	222	218	213		
196	209	193	192		
174	176	177	188	175	
		170			$T'(MoO_4)$ and δMo-O_b-Mo
152	156	148	156	153	
145	147	138	153	143	
					$T'(MoO_4)$ and δMo-O_b-Mo, $L(MoO_4)$, $L(Mo_2O_7)$,
128	136	130	140	133	$T'(Dy)$, $T'(Mo_2O_7)$, and τ_sOMo-MoO
114	122	115	124	107	
					$L(MoO_4)$, $L(Mo_2O_7)$, $T'(Dy)$, $T'(Mo_2O_7)$, and
96	108	102	121	80	τ_sOMo-MoO
87	98	89	112	66	
79	81	76	99	60	
66	73	62	81	53	
60	60	59	58	25	

of the Mo-O-Mo bridge are expected to be observed at about 275 cm^{-1} and 150 cm^{-1}, respectively. Our calculations also show that the lowest wave number modes, below 140 cm^{-1}, are strongly coupled and involve librations, torsions as well as translational motions of the Mo_2O_7 units and Dy atoms. A few representative vibrations of the Mo_2O_7 units are presented in Fig. 2.

It is worth noting that from Eq. (3), the $r(\nu)=-B\ln[(\nu-\nu_o)/A]$ relation can be obtained, which allows to estimate the bond compressibility for each Mo-O bond through the definition below[31,32]

$$\beta_x = -\left(\frac{1}{r}\frac{\partial r}{\partial P}\right)^{-1} = -\left(\frac{1}{r}\frac{\partial r}{\partial \nu}\frac{\partial \nu}{\partial P}\right)^{-1} = -\left(\frac{\alpha}{r}\frac{\partial r}{\partial \nu}\right)^{-1}, \quad (4)$$

where α is the slope coefficient for a respective mode obtained from wave number vs pressure plot. The estimated bond compressibilities so obtained are listed in Table V.

B. Pressure dependence of the Raman spectra

Pressure dependence of the Raman spectra of DMO is presented in the Figs. 3(a) and 4(a). Figures 3(b) and 4(b)

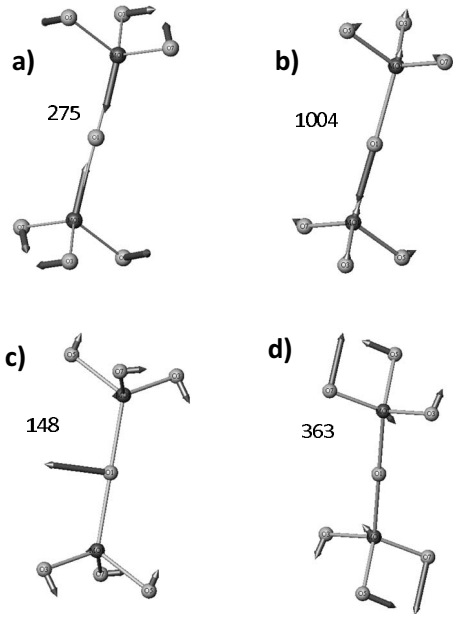

FIG. 2. Representative eigenvectors for some internal vibrations of the Mo_2O_7 units: (a) ν_sMo-O_b (A_g, 275 cm^{-1}), (b) ν_{as}Mo-O_b (A_u, 1004 cm^{-1}), (c) δMo-O_b-Mo (A_u, 148 cm^{-1}), and δMoO_3 (A_g, 363 cm^{-1}); ν means stretching vibration and δ means bending vibration.

show ω vs P plots for all observed modes. The wave number values were obtained by Lorentzian deconvolution of the Raman spectra. The slope curve coefficients (α) were obtained by linear fittings using the relation $\omega=\omega+\alpha P$.

Wave numbers of the observed modes and respective α coefficients are summarized in Table VI. The obtained data show that in the 0–2.0 GPa range majority of modes shift linearly toward higher wave numbers with increasing pressure [Fig. 4(b)]. This is an expected behavior since the ionic

TABLE V. List of bond compressibility related to each Mo-O stretching mode for the ambient phase (phase I) and high-pressure phase (phase II) estimated according to Eq. (4).

Phase I		Phase II	
ω (cm^{-1})	β_x (GPa^{-1})	ω (cm^{-1})	β_x (GPa^{-1})
970	39	974	136
952	42	958	121
941	51	946	98
859	62	929	64
844	28	877	47
837	23	863	77
835	30	849	59
813	23	841	38
793	26	819	41
783	22	794	22
		770	23
		721	3

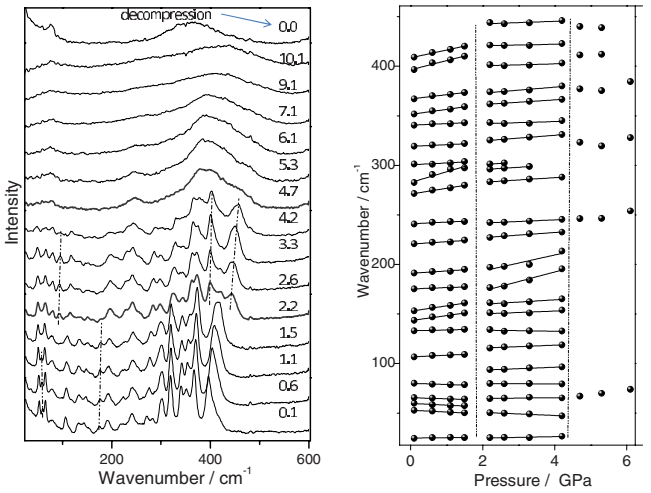

FIG. 3. (Color online) (a) Raman spectra of DMO recorded at different pressures during compression experiments (low wavenumber region). The numbers over the spectra are the respective pressures in units gigapascal. (b) Wave number vs pressure plots of the Raman modes observed in DMO crystal (20–500 cm^{-1} range) for compression experiment. The vertical lines indicate the pressure at which DMO undergoes a phase transition and PIA. The solid lines are linear fits on the data to $\omega(P)=\omega_0\alpha P$.

distances decrease as the pressure increases.[33] However, it is worth noting that a number of modes below 100 cm^{-1} exhibit negative α slope values [see Fig. 3(b) and Table VI]. This behavior has been also observed for $Gd_2(MoO_4)_3$.[12] In DMO system these modes correspond to Dy translations, tetrahedral librations, and Mo translations. Negative slope can be most likely attributed to transverse bond motions.[34] These modes contribute to negative Grüneisen parameters and lead to an increase in anharmonicity degree in crystals.

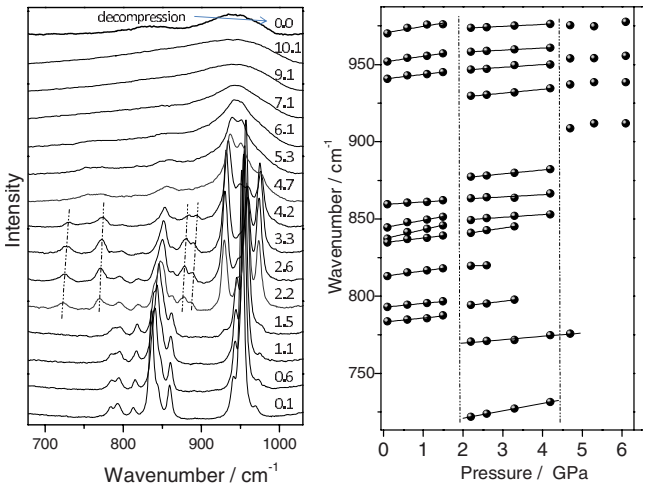

FIG. 4. (Color online) (a) Raman spectra of DMO recorded at different pressures during compression experiments (high wavenumber region). The numbers over the spectra are the respective pressures in gigapascal. (b) Wave number vs pressure plots of the Raman modes observed in DMO crystal (700–1000 cm^{-1} range) for compression experiment. The vertical lines indicate the pressure at which DMO undergoes a phase transition and PIA. The solid lines are linear fits on the data to $\omega(P)=\omega_0+\alpha P$.

TABLE VI. Experimental wave numbers (ω) along with their pressure slope coefficients (α).

Observed	
Phase I ($P2_1/c$) $\omega(\text{cm}^{-1})/\alpha(\text{cm}^{-1}\ \text{GPa}^{-1})$	Phase II $\omega(\text{cm}^{-1})/\alpha(\text{cm}^{-1}\ \text{GPa}^{-1})$
970/4.3	974/1.26
952/3.8	958/1.35
941/3	946/1.6
859/1.7	929/2.3
844/3.4	877/2.5
837/4.1	863/1.4
835/3	849/1.7
813/3.4	841/2.5
793/2.5	819/1.96
783/2.6	794/3.0
	770/0.22
	721/4.0
409/7.9	440/1.2
396/9.3	419/0.8
367/4.3	399/1.0
351/5.1	367/3.0
340/0.8	357/2.4
319/1.7	340/1.1
301/1.9	319/2.9
	291/2.4
283/10	278/2.3
271/5.9	
	238/1.6
241/1.8	222/2.6
221/2.4	200/−0.7
191/2.4	160/7.1
175/1.4	155/2.2
153/5.4	147/1.4
143/5.1	135/−0.5
133/0.9	113/1.5
107/1.8	90/1.5
	80/−0.2
80/−1.1	64/0.3
66/−1.2	
60/−1.8	54/−1.6
53/−1.9	23/0.7
25/0.4	

At about 2.0 GPa a number of changes are observed in the spectra. For instance, clear jumps are observed for the 409, 301, 970, and 844 cm^{-1} modes. Changes in ω vs P slope can also be noticed for the modes at 837 and 175 cm^{-1}. Another characteristic feature is appearance of new modes at 877, 929, 770, 443, 400, and 93 cm^{-1}. These changes strongly suggest that DMO experiences a structural phase transition at about 2 GPa. The new phase is stable up to 4.3 GPa and above this pressure a new set of changes can be noticed in the Raman spectra. In particular, at 4.7 GPa the bands broaden significantly giving rise to broad bands. These changes indicates onset of a PIA. The loss of long-range order increases gradually. At 7.1 GPa resolved bands are no longer observed in the spectra but the spectrum consists of only two very broad contours at approximately 400 and 960 cm^{-1}. This result points to complete amorphization of the sample at this pressure.

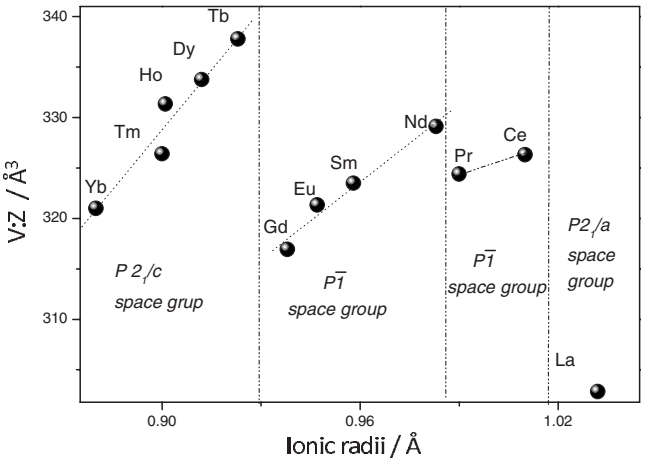

FIG. 5. Unit-cell volume per molecule unit for different $Ln_2Mo_4O_{15}$ systems as a function of ionic radii (Refs. 7 and 35). Dotted lines are guide for eyes.

Let us now discuss the possible structural changes that occur at the phase transition at around 2.0 GPa. One of the possibility is that the high-pressure phase of DMO has the same structure as the ambient pressure phase of $La_2Mo_4O_{15}$ (structural type I, $P2_1/n$ space group), $Ce_2Mo_4O_{15}$ or $Pr_2Mo_4O_{15}$ (structural type II, $P\bar{1}$ space group), or $Ln_2Mo_4O_{15}$ for Ln=Nd-Gd (structural type III, $P\bar{1}$ space group). Using the available literature data we have plotted in the Fig. 5 the dependence of the unit-cell volume per $Ln_2Mo_4O_{15}$ formula (V/Z) as a function of ionic radii for some lanthanide molybdates.[35] The presented diagram shows that the structural types I, II, and III have smaller V/Z values than that found for DMO. Therefore, considering only this factor high-pressure transition could lead to any of these denser phases. However, closer inspection of the crystal structures for $Ln_2Mo_4O_{15}$ systems shows that they have very different structural arrangement. $La_2Mo_4O_{15}$ (type I) consists of Mo_6O_{22} units composed of two MoO_6 octahedra sharing vertices with four MoO_4 tetrahedra. The Ce and Pr molybdates (type II) contain $(Mo_4O_{14})_\infty$ units, which are built up from edge-shared MoO_6 octahedra and MoO_4 tetrahedra. The structural type III is very complicated since it contains both $(Mo_4O_{17})_\infty$ and MoO_4 units. The $(Mo_4O_{17})_\infty$ units are built up from corner-shared MoO_6 octahedra and edge-shared MoO_5 trigonal bipyramids. In contrast to other $Ln_2Mo_4O_{15}$ compounds, the structure of DMO (type IV) is quite simple since the main building block is one Mo_2O_7 unit that is weakly connected to two MoO_4 tetrahedra. The distance between different Mo_2O_7 units is large and therefore it is not very likely that this structure could transform to type I, II, or III at relatively low pressure of 2.2. GPa since such transfor-

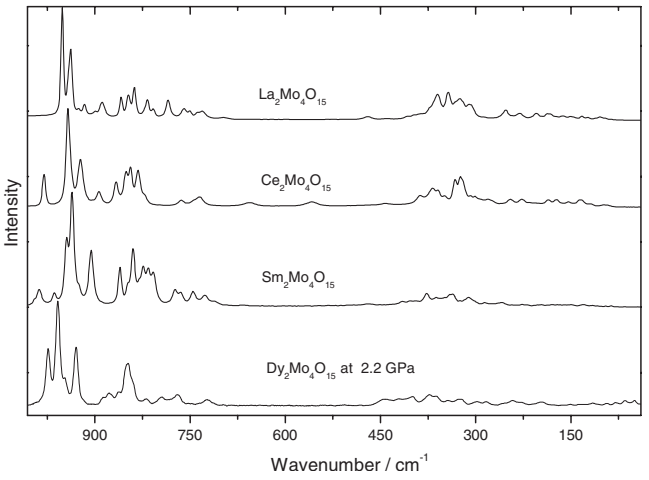

FIG. 6. Comparison of the Raman spectrum of $Dy_2Mo_4O_{15}$ at 2.2 GPa and the spectra of three representative molybdates crystallizing in structural type I ($La_2Mo_4O_{15}$), II ($Ce_2Mo_4O_{15}$), and III ($Sm_2Mo_4O_{15}$).

mation would require very large reconstruction of the structure in order to create larger molybdenum-oxygen units. This conclusion is supported by our Raman study of three representative compounds crystallizing in the structural type I, II, and III (see Fig. 6). As can be noticed the spectra of the measured compounds are different from the spectrum of DMO at 2.2 GPa. This result proves that the high-pressure structure of DMO is different from any known ambient pressure structure of $Ln_2Mo_4O_{15}$.

The obtained results show that the phase transition at 2.2 GPa is associated with strong structural changes within the Mo_4O_{15} units and Dy-O polyhedra. The two characteristic features of this transformation are (i) increase in the number of observed Raman features from 32 at ambient pressure to 35 at 2.2 GPa, (ii) appearance of new stretching modes at 721 and above 900 cm^{-1}, and (iii) negative shift of the highest wave number mode at the phase transition. Table IV shows that there should be 14 Raman active stretching modes for the ambient pressure DMO phase but only ten bands could be observed due to small Davydov splitting into A_g and B_g components. Therefore, small increase in the number of bands at the phase transition can be most likely attributed to increase in the Davydov splitting without any change in the number of atoms in the unit cell. The appearance of new mode at 721 cm^{-1} indicates that some of the Mo-O bonds became significantly longer. Figure 6 shows that when structure is built up of edge-shared MoO_6 octahedra, like in $Ce_2Mo_4O_{15}$ structure, some bands should be observed in the 700–500 cm^{-1} range. No bands in this range are, however, observed for $Sm_2Mo_4O_{15}$ (type III) or $La_2Mo_4O_{15}$ (type I), which consist of corner-shared octahedra and edge-shared trigonal bipyramids (type III) or corner-shared MoO_6 octahedra and MoO_4 tetrahedra (type I). We conclude, therefore, that the high-pressure structure of DMO does not contain any edge-shared octahedra and the coordination of the Mo atoms may increase to pentagonal. This assumption is very plausible since in the ambient pressure phase the MoO_4 and Mo_2O_7 units are not well separated [the distance between one of the oxygen atoms of the MoO_4 group and the Mo atom of the Mo_2O_7 group is 2.514 Å for the isostructural $Ho_2Mo_4O_{15}$ (Ref. 35)]. The application of pressure may easily decrease this distance and when pressure reaches 2.2 GPa, a sudden reorientation of the MoO_4 groups in respect to the Mo_2O_7 groups occurs, which leads to formation of more compact molybdenum-oxygen coordination. As we can see in Table V, this conclusion is consistent with higher calculated bond compressibilities for the phase above 2.2 GPa when compared to the value obtained for the ambient pressure phase. It is also consistent with former studies of $Gd_2(MoO_4)_3$ molybdate, which showed negative shift of the highest wave-number stretching modes and appearance of new stretching modes at lower wave numbers at the pressure-induced phase transition due to change in the coordination around Mo atoms from 4 to 5 at about 3.1 GPa.[12]

C. Amorphization process

Amorphization of DMO starts already at about 4.2 GPa and at the highest pressure reached in the experiment (10.1 GPa) only two very broad contours are observed at approximately 440 and 960 cm^{-1}. Upon releasing pressure the spectrum of the starting orthorhombic phase was not recovered, i.e., we observed only very broad bands, which are very similar to those observed at high pressures. This result points to irreversibility of the amorphization process.

As mentioned above, it is widely accepted in the literature that the amorphous process are originated from three different mechanisms, namely: (i) mechanical deformation, (ii) chemical decomposition, or (iii) kinetic hindrance of equilibrium phase transitions to another crystalline structure.[10–12] The first process (mechanical) is related to nonhomogeneous macroscopic deformation of the crystal by nonhydrostatic shear component. In this case, the process results in a reminiscent short range and the original crystal structure can be recovered after releasing pressure. Irreversibility of the DMO amorphization process is not compatible with this scenario. Furthermore, our experiments were performed at hydrostatic conditions. The second mechanism, chemical decomposition, leads the initial complex compound to simpler products. This mechanism is favored if the component product occupy smaller volume than the parent crystal. It is important to note that neither mechanical nor chemical decomposition process lead to a new thermodynamic state of the system, in contrast to kinetically hindered phase transition, the third amorphization process. This mechanism leads the system to a disordered structure but without changes in the initial chemical bonds. In this case the final disordered state can be considered as a new thermodynamic state (stable or metastable) resulting from the hindrance of a crystal to crystal phase transition. The irreversibility of the amorphization process observed in our experiment is consistent with either chemical decomposition or kinetically hindered phase transition.

By analyzing the Raman spectra, we can see that the behavior of DMO under applied pressure is similar to that observed for $Gd_2Mo_3O_{12}$, i.e., both systems present a number of modes with negative pressure slope coefficients below 100 cm^{-1}, and there is a marked similarity between the

broad bands at around 950 cm^{-1} indicating the existence of short Mo-O bonds after amorphization.[12] As mentioned above, reports on pressure-induced decomposition of $Ln_2Mo_3O_{12}$ systems into a mixture of simple oxides at high temperature and high pressure, and the observation of PIA at ambient temperature suggest that in these systems PIA could arise from the kinetic hindrance of an equilibrium decomposition.[11,14,15] Since the structural motif of $Ln_2Mo_3O_{12}$ and $Ln_2Mo_4O_{15}$ systems are not very different, the hypothesis of decomposition must be considered for DMO. It was reported for related $Nd_2Mo_4O_{15}$ neodymium molybdate that $Nd_6Mo_{10}O_{39}$ is a nonequilibrium phase (metastable phase) which presumably occurs along the pathway,[1]

$$3Nd_2Mo_4O_{15} \rightarrow Nd_6Mo_{10}O_{39} + 2MoO_3 \rightarrow 3Nd_2(MoO_4)_3 + 3MoO_3.$$

It is necessary, for decomposition to occur at high pressure that the total volume of the daughter phases must be smaller than that of the parent phase. Following the above diagram, the volume per $3Nd_2Mo_4O_{15}$ formulas of the final daughter phase $[3Nd_2(MoO_4)_3+3MoO_3]$ is 15% higher than the volume of the parent phase. However, for the metastable phase $(Nd_6Mo_{10}O_{39}+2MoO_3)$, the volume of daughter phase is 5% smaller than the volume of the parent phase.[1] Having this in mind, the $Dy_6Mo_{10}O_{39}$ metastable phase is a good candidate for the product of decomposition of this kind of system. It is worth to note, however, that decomposition of DMO into $Dy_2O_3+4MoO_3$ is even more favorable since in this case the volume of the daughter phase is 20.4% smaller than the volume of the parent phase. MoO_3 exhibits characteristic Raman peaks at 667 and 817 cm^{-1} that are not observed in our Raman spectra above 4.0 GPa.[36] The lack of these bands can be attributed to not sufficient kinetics at ambient temperature and therefore the appearance of daughter compounds in the form of a disordered assemblage of macroscopic phases is not expected to occur.[16] At ambient temperature the initiation of the process of decomposition at atomic or microscopic level eventually results in the amorphous phase.

On the basis of the obtained results we can propose that the mechanism of the PIA process in DMO is similar to that reported for $Zr(WO_4)_2$. The equilibrium phase is most likely $MoO_3+Dy_2O_3$ and the high-pressure phase II is the metastable phase. In the ambient pressure phase, the distance between one of the oxygen atoms of the MoO_4 group and the Mo atom of the Mo_2O_7 group is relatively short [for the isostructural $Ho_2Mo_4O_{15}$ this distance is only 2.514 Å (Ref. 35)]. Similar as in $Zr(WO_4)_2$,[37] the compression of the crystal would result in a repulsive contribution to the total energy and the structure would be sterically constrained. The increase in pressure leads to an increase in repulsive forces among oxygen atoms and to relieve this repulsion, the structure transforms into the high-pressure phase with more distorted polyhedra and higher coordination of Mo atoms. Further increase in pressure leads again to an increase in repulsive forces and destabilization of the structure, which results in the observed PIA. Our results indicate, therefore, that $Ln_2Mo_4O_{15}$ compounds constitute another group of molybdates, which may exhibit PIA phenomenon due to kinetically hindered chemical decomposition caused by steric constraints, as discovered previously for a number of $M^{IV}(M^{VI}O_4)_2$ and $M_2^{III}(M_{VI}O_4)_3$ molybdates and tungstates (M^{IV}=Zr,Hf; M^{III}=lanthanide,Y,Sc; and M^{VI}=Mo,W).[11–15,37–42]

IV. CONCLUSIONS

DMO was investigated by high-pressure Raman scattering and lattice-dynamics calculations. The assignment of modes was made based on LD calculation for the monoclinic structure. We observed two set of modifications in the Raman spectra at around 2.0 and 4.7 GPa. The modifications observed at 2.0 GPa are attributed to a structural phase transition, which leads to increase in Mo coordination. The bond compressibility, related to each Mo-O bond, were estimated for both the $P2_1/c$ and high-pressure phase. The modifications observed above 4.7 GPa indicate that the system transformed to an amorphous phase. This process is irreversible and low pressure of this transformation indicates that this process is intrinsic to the system and not due to nonhydrostatic stresses. Our analysis of volumetric transformation suggests that the PIA in DMO is mostly likely originated from a decomposition process.

ACKNOWLEDGMENTS

The Brazilian authors acknowledge financial support from CNPq, CAPES, FUNCAP, and FINEP agencies.

*Corresponding author; wparaguassu@pq.cnpq.br

[1] R. S. Barker and I. R. Evans, J. Solid State Chem. **179**, 1918 (2006).
[2] F. Dubois, F. Goutenoire, Y. Laligant, E. Suard, and P. Lacorre, J. Solid State Chem. **159**, 228 (2001).
[3] H. Naruke and T. Yamase, J. Solid State Chem. **173**, 407 (2003).
[4] H. Naruke and T. Yamase, Acta Crystallogr., Sect. E: Struct. Rep. Online **57**, 106 (2001).
[5] V. A. Efremov, N. N. Davydova, L. Z. Gokhman, A. A. Evdokimov, and V. K. Trunov, Zh. Neorg. Khim. **33**, 3005 (1988).
[6] V. A. Efremov, N. N. Davydova, and V. K. Trunov, Zh. Neorg. Khim. **33**, 3001 (1988).
[7] L. Sebastian, S. Sumithra, J. Manjanna, A. M. Umarji, and J. Gopalakrishnan, Mater. Sci. Eng., B **103**, 289 (2003).
[8] R. J. Speedy, J. Phys.: Condens. Matter **8**, 10907 (1996).
[9] C. A. Perottoni and J. A. H. da Jornada, Science **280**, 886 (1998).
[10] R. J. Hemley, A. P. Jephcoat, H. K. Mao, L. C. Ming, and M. H. Manghnani, Nature (London) **334**, 52 (1988).
[11] A. K. Arora, Solid State Commun. **115**, 665 (2000).

[12] G. Lucazeau, P. Bouvier, A. Pasturel, O. Le Bacq, and T. Pagnier, Acta Phys. Pol. A **116**, 25 (2009).
[13] V. Dmitriev, V. Sinitsyn, R. Dilanian, D. Machon, A. Kuznetsov, E. Ponyatovsky, G. Lucazeau, and H. P. Weber, J. Phys. Chem. Solids **64**, 307 (2003).
[14] G. Richard and P. Richet, Geophys. Res. Lett. **17**, 2093 (1990).
[15] F. Guyot and B. Reynard, Chem. Geol. **96**, 411 (1992).
[16] T. R. Ravindran, K. A. Akhilesh, and T. A. Mary, J. Phys.: Condens. Matter **13**, 11573 (2001).
[17] J. S. O. Evans, Z. Hu, J. D. Jorgensen, D. N. Argyriou, S. Short, and A. W. Sleight, Science **275**, 61 (1997).
[18] J. S. O. Evans, T. A. Mary, and A. W. Sleight, J. Solid State Chem. **133**, 580 (1997).
[19] T. A. Mary, J. S. O. Evans, A. W. Sleight, and T. Vogt, Science **272**, 90 (1996).
[20] D. V. S. Muthu, B. Chen, J. M. Wrobel, A. M. K. Andersen, S. Carlson, and M. B. Kruger, Phys. Rev. B **65**, 064101 (2002).
[21] B. Chen, D. V. S. Muthu, Z. X. Liu, A. W. Sleight, and M. B. Kruger, Phys. Rev. B **64**, 214111 (2001).
[22] A. M. Amado and P. J. A. Ribeiro-Claro, J. Mol. Struct.: THEOCHEM **469**, 191 (1999).
[23] J. D. Gale, J. Chem. Soc., Faraday Trans. **93**, 629 (1997).
[24] E. Dowty, Phys. Chem. Miner. **14**, 67 (1987).
[25] G. D. Saraiva, W. Paraguassu, M. Maczka, P. T. C. Freire, J. A. Lima, C. W. A. Paschoal, J. Mendes, and A. G. Souza, J. Raman Spectrosc. **39**, 937 (2008).
[26] M. Maczka, J. Hanuza, W. Paraguassu, A. G. Souza, P. T. C. Freire, and J. M. Filho, Appl. Phys. Lett. **92**, 112911 (2008).
[27] W. Paraguassu, A. G. Souza, M. Maczka, P. T. C. Freire, F. E. A. Melo, J. Mendes, and J. Hanuza, J. Phys.: Condens. Matter **16**, 5151 (2004).
[28] W. Paraguassu, M. Maczka, A. G. Souza, P. T. C. Freire, F. E. A. Melo, and J. Mendes, Vib. Spectrosc. **44**, 69 (2007).
[29] M. M. Wu, Y. Z. Cheng, J. Peng, X. L. Xiao, Z. B. Hu, Y. T. Liu, and D. F. Chen, Mater. Chem. Phys. **113**, 451 (2009).
[30] F. D. Hardcastle and I. E. Wachs, J. Phys. Chem. **95**, 10763 (1991).
[31] R. M. Hazen and H. Yang, Am. Mineral. **84**, 1956 (1999).
[32] A. M. Hofmeister and H. Mao, Geophysics **99**, 564 (2001).
[33] R. M. Hazen and C. T. Prewitt, Am. Mineral. **62**, 309 (1977).
[34] W. Miller, C. W. Smith, D. S. Mackenzie, and K. E. Evans, J. Mater. Sci. **44**, 5441 (2009).
[35] Inorganic Crystal Structure Database (ICSD), 2010.
[36] D. Liu, W. W. Lei, J. Hao, D. D. Liu, B. B. Liu, X. Wang, X. H. Chen, Q. L. Cui, G. T. Zou, J. Liu, and S. Jiang, J. Appl. Phys. **105**, 023513 (2009).
[37] S. K. Sikka, J. Phys.: Condens. Matter **16**, S1033 (2004).
[38] T. Sakuntala, R. Rao, A. B. Garg, S. N. Achary, and A. K. Tyagi, J. Appl. Phys. **104**, 063506 (2008).
[39] K. Sakai and M. Tani, J. Appl. Phys. **97**, 1 (2005).
[40] G. D. Mukherjee, A. S. Karandikar, V. Vijayakumar, B. K. Godwal, S. N. Achary, A. K. Tyagi, A. Lausi, and E. Busetto, J. Phys. Chem. Solids **69**, 35 (2008).
[41] N. Garg, K. K. Pandey, C. Murli, K. V. Shanavas, B. P. Mandal, A. K. Tyagi, and S. M. Sharma, Phys. Rev. B **77**, 214105 (2008).
[42] T. Varga and A. P. Wilkinson, Phys. Rev. B **79**, 224119 (2009).